

**Fax to: +44 870 762 8807 (UK) or
+91 44 4208 9499 (INDIA)**



**From: Springer Correction Team
6&7, 5th Street, Radhakrishnan Salai, Chennai, Tamil Nadu, India – 600 004**

**Re: Journal of Materials Science DOI: 10.1007/s10853-007-1512-2
Growth of boride layers on the 13% Cr steel surface in a mixture of amorphous
boron and KBF₄**

Authors: V. Dybkov

I. Permission to publish

I have checked the proofs of my article and

- I have **no corrections**. The article is ready to be published without changes.
- I have **a few corrections**. I am enclosing the following pages:
- I have made **many corrections**. Enclosed is the **complete article**.

Date / signature _____

II. Copyright Transfer Statement (sign only if not submitted previously)

The copyright to this article is transferred to Springer Science+Business Media, LLC
(for government employees: to the extent transferable) effective if and when the article is accepted for publication. The author warrants that his/her contribution is original and that he/she has full power to make this grant. The author signs for and accepts responsibility for releasing this material on behalf of any and all co-authors. The copyright transfer covers the exclusive right to reproduce and distribute the article, including reprints, translations, photographic reproductions, microform, electronic form (offline, online) or any other reproductions of similar nature.

An author may self-archive an author-created version of his/her article on his/her own website and his/her institution's repository, including his/her final version; however he/she may not use the publisher's PDF version which is posted on www.springerlink.com. Furthermore, the author may only post his/her version provided acknowledgement is given to the original source of publication and a link is inserted to the published article on Springer's website. The link must be accompanied by the following text: "The original publication is available at www.springerlink.com."

The author is requested to use the appropriate DOI for the article (go to the Linking Options in the article, then to OpenURL and use the link with the DOI). Articles disseminated via www.springerlink.com are indexed, abstracted and referenced by many abstracting and information services, bibliographic networks, subscription agencies, library networks, and consortia.

After submission of this agreement signed by the corresponding author, changes of authorship or in the order of the authors listed will not be accepted by Springer.

Date / Author's signature _____

ELECTRONIC REPRINT ORDER FORM

After publication of your journal article, electronic (PDF) reprints may be purchased by arrangement with Springer and Aries Systems Corporation.

The PDF file you will receive will be protected with a copyright system called DocuRights®. Purchasing 50 reprints will enable you to redistribute the PDF file to up to 50 computers. You may distribute your allotted number of PDFs as you wish; for example, you may send it out via e-mail or post it to your website. You will be able to print five (5) copies of your article from each one of the PDF reprints.

Please type or print carefully. Fill out each item completely.

1. Your name: _____
 Your e-mail address: _____
 Your phone number: _____
 Your fax number: _____
2. Journal title (vol, iss, pp): _____
3. Article title: _____
4. Article author(s): _____
5. How many PDF reprints do you want? _____
6. Please refer to the pricing chart below to calculate the cost of your order.

Number of PDF reprints	Cost (in U.S. dollars)
50	\$200
100	\$275
150	\$325
200	\$350

NOTE: Prices shown apply only to orders submitted by individual article authors or editors. Commercial orders must be directed to the Publisher.

All orders must be prepaid. Payments must be made in one of the following forms:

- a check drawn on a U.S. bank
- an international money order
- Visa, MasterCard, or American Express (no other credit cards can be accepted)

PAYMENT (type or print carefully):

Amount of check enclosed: _____ (payable to Aries Systems Corporation)

VISA _____

MasterCard _____

American Express _____

Expiration date: _____ Signature: _____

Print and send this form with payment information to:

Aries Systems Corporation
 200 Sutton Street
 North Andover, Massachusetts 01845
 Attn.: Electronic Reprints
 — OR —
 Fax this to Aries at: 978-975-3811

Your PDF reprint file will be sent to the above e-mail address. If you have any questions about your order, or if you need technical support, please contact: support@docurights.com

For subscriptions and to see all of our other products and services, visit the Springer website at:
<http://www.springeronline.com>

HOW TO USE THE CORRECTION GRID

- [1] Put the page number of each correction in the Page Number column.
- [2] Put the line numbers of each correction in the Line Number column.
- [3] Write the number of the equation, table or figure that needs correction in the Equation Number, Table Number or Figure Number columns.
- [4] Insert the text/symbols you wish to be changed in the Incorrect column.
- [5] Insert the correct text/symbols in the Correct column. If you include extra text/symbols here, indicate the exact items that need to be changed by highlighting them in the color red (for example ‘The outer membrane surface...’ corrected to ‘The outer membrane surface...’).
- [6] Our typesetter queries on the galley proof regarding insufficient information or required clarifications will already be inserted into the grid (in the Page Number, Line Number and Incorrect columns). Please answer these queries by putting the relevant information in the Correct column. If you are unable to answer a query, indicate this by putting the letters ‘NA’ in the Correct column.
- [7] New versions of figures/tables can be included as an ‘attachment’ to the Correction Grid e-mail.
- [8] If you need to add more rows to the grid, press the TAB key on your keyboard when you are in the last row.
- [9] The Correction Grid is a basic Microsoft Word table. If you do not use Microsoft Word, please return corrections in RTF format similar to the example provided below.

Example of how to use the correction grid

MANUSCRIPT I.D.: ABCD 1234

Page Number	Line Number	Equation Number	Table Number	Figure Number	Incorrect	Correct	Not for Author use
1	16				Sith	Smith	
5			3		Caption: Amount of CO inhalation person	Caption: Amount of CO inhalation per person	
7				4	Replace figure with new one on attachment to this e-mail		
10		19			X (X-1)	X (Y-1)	

Metadata of the article that will be visualized in OnlineFirst

ArticleTitle	Growth of boride layers on the 13% Cr steel surface in a mixture of amorphous boron and KBF_4	
Article Sub-Title		
Journal Name	Journal of Materials Science	
Corresponding Author	Family Name	Dybkov
	Particle	
	Given Name	V. I.
	Suffix	
	Division	Department of Physical Chemistry of Inorganic Materials
	Organization	Institute for Problems of Materials Science
	Address	03180, Kyiv, Ukraine
	Email	vdybkov@ukr.net
Schedule	Received	18 March 2006
	Revised	
	Accepted	9 January 2007
Abstract	<p>Two borides FeB and Fe_2B were found to form as separate layers at the interface between a 13% Cr steel and boron at 850–950 °C and reaction times up to 12 h. The average chromium content is 8 at.% in the FeB layer and 9 at.% in the Fe_2B layer. Both layers are characterized by a pronounced texture. The strongest reflections are {002} and {020} for the orthorhombic FeB phase and {002} for the tetragonal Fe_2B phase. Diffusional growth kinetics of boride layers are close to parabolic and can alternatively be described by a system of two non-linear differential equations, producing a good fit to the experimental data. Annealing of a borided steel sample in the absence of boriding media results in disappearance of the FeB layer. Microhardness values are 17.9 ± 1.5 GPa for the FeB layer, 16.1 ± 0.9 for the Fe_2B layer and 5.9 ± 0.3 GPa for the steel base. The abrasive wear resistance of the FeB layer is 25 times greater than that of the steel base. The Fe_2B layer yields about a 15-fold increase in wear resistance of steel samples.</p>	
Footnote Information		

3 Growth of boride layers on the 13% Cr steel surface in a mixture 4 of amorphous boron and KBF_4

5 V. I. Dybkov

6 Received: 18 March 2006 / Accepted: 9 January 2007 / Published online: ■
7 © Springer Science+Business Media, LLC 2007

8 **Abstract** Two borides FeB and Fe_2B were found to form
9 as separate layers at the interface between a 13% Cr steel
10 and boron at 850–950 °C and reaction times up to 12 h.
11 The average chromium content is 8 at.% in the FeB layer
12 and 9 at.% in the Fe_2B layer. Both layers are characterized
13 by a pronounced texture. The strongest reflections are
14 {002} and {020} for the orthorhombic FeB phase and
15 {002} for the tetragonal Fe_2B phase. Diffusional growth
16 kinetics of boride layers are close to parabolic and can
17 alternatively be described by a system of two non-linear
18 differential equations, producing a good fit to the experi-
19 mental data. Annealing of a borided steel sample in the
20 absence of boriding media results in disappearance of the
21 FeB layer. Microhardness values are 17.9 ± 1.5 GPa for the
22 FeB layer, 16.1 ± 0.9 for the Fe_2B layer and 5.9 ± 0.3 GPa
23 for the steel base. The abrasive wear resistance of the FeB
24 layer is 25 times greater than that of the steel base. The
25 Fe_2B layer yields about a 15-fold increase in wear resis-
26 tance of steel samples.

29 Introduction

30 Boriding is one of the widespread thermochemical
31 surface treatments used to improve mechanical and cor-
32 rosive wear resistance, hardness and other service char-

acteristics of metals, alloys and steels [1–3]. Iron borides 33
 Fe_2B and FeB exist in the Fe–B binary system [4–7]. 34
Therefore, with iron, its alloys and steels, either one- 35
phase or two-phase coatings can be obtained, depending 36
on boriding media employed and temperature-time con- 37
ditions of a boriding procedure. 38

Note that even if three or more compounds exist in the 39
metal-boron binary system, in most cases only two of them 40
form separate layers at the interface between reacting 41
phases [8]. This contradicts diffusional considerations [9] 42
predicting the simultaneous formation and subsequent 43
parabolic growth of the layers of all compounds of any 44
binary system, whatever their number, but agrees with a 45
physicochemical viewpoint [10], according to which one or 46
two layers can occur and grow simultaneously under con- 47
ditions of diffusion control, with other compound layers 48
being skipped for kinetic reasons. 49

Boriding at 950 °C for 6 h in a mixture of 30% SiC and 50
70% $\text{Na}_2\text{B}_4\text{O}_7$ is known to produce a coating of a thickness 51
of 15 μm on the surface of the 30×13 (0.30% C and 52
13% Cr) steel material [11], similar to that material 53
employed in this investigation. With a mixture of 30– 54
35% B_4C and 70–65% $\text{Na}_2\text{B}_4\text{O}_7$ and the $\text{Na}_2\text{B}_4\text{O}_7$ melt 55
(electrolysis), appropriate thickness values are 40 and 56
55 μm , respectively. Mixtures of amorphous boron and 57
 KBF_4 appear to be more effective boriding agents due to 58
the formation of a gas phase (mainly BF_3) at elevated 59
temperatures [1, 8, 11]. In this work, the results of inves- 60
tigation of the interaction of a commercial 40×13 steel 61
and boron in a mixture of amorphous boron powder and 62
5% KBF_4 at 850–950 °C are presented, with the main 63
emphasis on establishing the boride layer-growth kinetics 64
that received comparatively little attention. Also, the 65
results of dry abrasive wear resistance tests of boride 66
coatings formed on the steel-material surface are presented. 67

A1 V. I. Dybkov (✉)
A2 Department of Physical Chemistry of Inorganic Materials,
A3 Institute for Problems of Materials Science,
A4 Kyiv 03180, Ukraine
A5 e-mail: vdybkov@ukr.net

68 **Experimental procedure**69 **Materials and specimens**

70 The materials used included a 40 × 13 steel rod (16 mm
71 diameter) in the as-received condition (without any addi-
72 tional heat treatment), amorphous boron and analytical-
73 grade KBF₄. The content of main components of the steel
74 was 85.2% Fe, 13.6% Cr, 0.38% C, 0.30% Mn, 0.30% Si
75 and 0.20% Ni. All contents are given in mass percent if
76 otherwise not stated. The steel microstructure consisting of
77 the body centered cubic α -phase (ferrite) and carbides
78 Me₂₃C₆ (Me = Cr, Fe) is shown in Fig. 1.

79 Initially, the boron powder contained 98.3% B, 0.04% C,
80 1.6% O and insignificant amounts of Si, Cu, Mg (< 0.01%
81 each) and Fe (< 0.001%). Before the boriding experiments,
82 the powder was first heated slowly in vacuum up to 1,450 °C
83 and then calcined at this temperature for 2 h in an atmo-
84 sphere of argon at a pressure of 2.5 × 10⁴ Pa to remove
85 volatile oxides. Subsequently, it was cooled by filling the
86 chamber with argon at atmospheric pressure. The average
87 cooling rate (to 200–250 °C) was around 2 °C s⁻¹. After this
88 treatment, no significant changes of the powder morphology
89 and structure were revealed, except for the beginning of
90 resolution of some broad X-ray diffraction peaks. KBF₄ was
91 preliminarily dried in steps at 95, 110, 130 and 170 °C (24 h at
92 each temperature).

93 Specimens in the form of Tablets, 11.28 mm diameter
94 and 5.5 mm high, were machined from the steel rod. Flat
95 sides (1 cm² area) of the Tablets were ground and polished
96 mechanically.

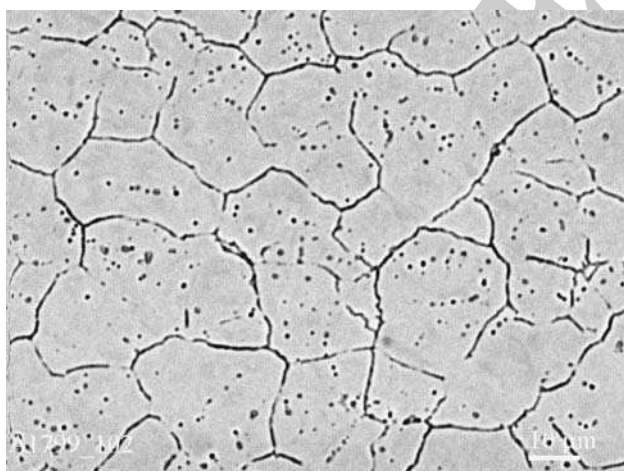


Fig. 1 The 13% Cr steel microstructure. Polished mechanically and etched for 60 s in a solution of 4 ml HF and 8ml HNO₃ in 100 ml ethanol at room temperature

Experimental methods

The vacuum device VPBD-2S employed for boriding steel samples has been described elsewhere [12]. The experiment was carried out in an alumina crucible, 13 mm inner diameter and 40 mm high.

A steel Tablet was embedded into a mixture of boron powder with 5% KBF₄ as an activator. This amount of KBF₄ appears to be optimum [1, 8]. The mixture was then slightly pressed, and a load of 8.5 g (a low-carbon steel cylinder) was placed on top. The crucible was closed with a low-carbon steel lid and placed into a steel-sheet holder, mounted to a guide rod capable of moving in the vertical direction.

The chamber was pumped to a pressure of about 10 Pa and filled with high-purity argon (99.999 vol.% Ar). This procedure was repeated twice. Then, the chamber was again pumped and filled with argon at a pressure of 2.5 × 10⁴ Pa, and heating was started. During heating, the crucible with its contents was in the cold zone above the furnace. After the required temperature in the range of 850–950 °C had been reached in the furnace, the crucible, pre-heated to about 400 °C, was moved into its middle part. After an initial drop, the temperature attained its pre-determined value in 4–5 min and was then maintained constant within ± 1 °C with the help of an automatic thermoregulator VRT-3. The temperature measurements were carried out using a Pt–PtRh thermocouple. The experiments were performed at temperatures of 850, 900 and 950 °C. Their duration was 3,600–43,200 s (1–12 h).

After the experiment, the steel Tablet coated with boride layers was cut along the cylindrical axis into two unequal parts (4 and 7 mm) using an electric-spark machine. The greater part of the Tablet was embedded into a cold-setting epoxy resin and used to prepare a metallographic cross-section. The lesser part was used for X-ray diffraction investigations (plain-view samples).

Characterization of the steel and boride layers was carried out with the help of metallography, X-ray (XA) and chemical (CA) analyses, and electron probe microanalysis (EPMA). The thickness of boride layers was measured using an optical microscope MIM-7 equipped with a HP Photosmart 720 camera. Eight to ten measurements were made at different places of the interface (~1 cm long on any cross-section) between the reacting phases and the average value of the layer thickness was found. The mean relative error of its determination was around ±12%.

The chemical composition of the layers and the concentration profiles of the elements in the steel-boron transition zone were obtained using electron probe microanalyzers JEOL Superprobe 733 and CAMECA

147 Camebax S $\times 50$. The beam spot diameter and the phase
148 volume analyzed at each point were estimated to be about 1
149 and $2 \mu\text{m}^3$, respectively.

150 X-ray diffraction patterns were taken immediately from
151 the surface of Tablet samples on a DRON-3 apparatus
152 using Cu K_α radiation. When taking the first pattern, no
153 polishing of a borided steel sample was applied (section 0).
154 Then, about $40 \mu\text{m}$ of a boride layer was removed by
155 grinding and subsequent polishing, and another X-ray dif-
156 fraction pattern was taken (section I). This procedure was
157 repeated at a step of $20\text{--}30 \mu\text{m}$ until the steel base was
158 reached (sections II-V). Six X-ray diffraction patterns were
159 thus taken on each borided steel sample.

160 Microhardness measurements on metallographic cross-
161 sections were carried out using a PMT-3 tester with the
162 diamond pyramide (Vickers indenter). The load was
163 0.98 N (100 g).

164 Abrasive wear resistance tests were carried out on P180
165 SiC emery paper tape (main fraction grain size $63 \mu\text{m}$,
166 maximum $90 \mu\text{m}$) using an AWRD-5 device. The velocity
167 of continuous movement of the tape (30 m long) was
168 0.35 m s^{-1} , while the gauge length during each test was
169 27.0 m . The load was 50 N (5.1 kg). The working area of
170 Tablet samples was 1 cm^2 .

171 The wear resistance was determined by means of
172 weighing the samples and measuring their height. The
173 accuracy of weighting measurements (analytical balance)
174 was $\pm 5 \times 10^{-5} \text{ g}$. The sample height was measured using

a micrometer ($\pm 0.005 \text{ mm}$). Layer-by-layer measurements
175 on the same borided sample allowed the wear character-
176 istics of different boride phases as well as the steel base to
177 be determined separately. 178

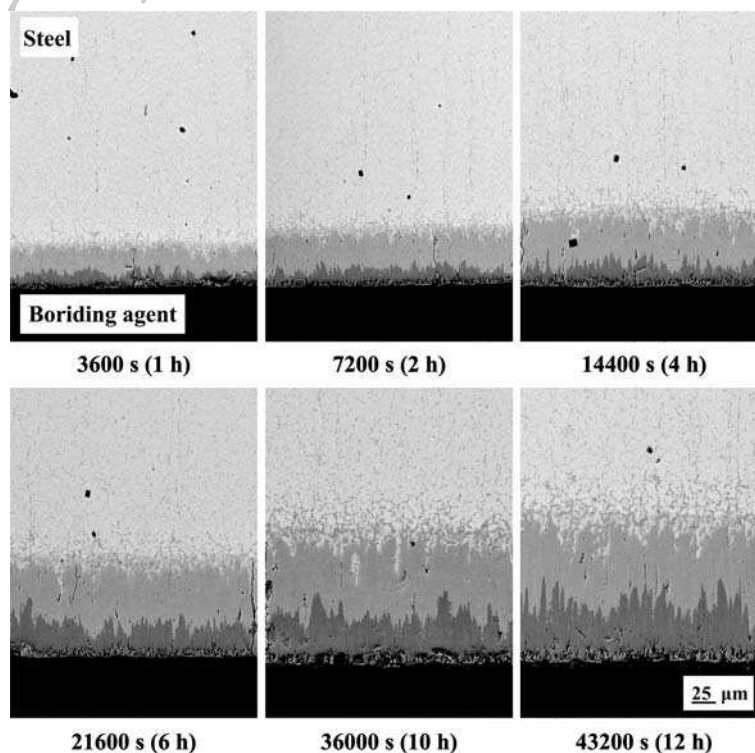
Results and discussion 179

Phase identity and chemical composition of boride
180 layers 181

Two boride phases were found to form as separate layers at
182 the steel-boron interface at $850\text{--}950 \text{ }^\circ\text{C}$ and reaction times
183 up to 12 h (Fig. 2). Layer-by-layer X-ray analysis (Fig. 3)
184 and a further comparison of our and literature [13] data
185 showed the outer layer bordering the boriding agent to be
186 the FeB phase (Fig. 4 and Table 1), while the inner layer
187 adjacent to the steel base to be the Fe_2B phase (Fig. 5 and
188 Table 2). 189

As seen from cross-sectional micrographs in Figs. 2 and 3,
190 both layers consist of columnar crystals oriented prefer-
191 entially in the direction of diffusion. Their characteristic
192 feature is a pronounced texture. The strongest reflections
193 are $\{002\}$ ($2\theta = 63.2^\circ$ and spacing, $d = 0.148 \text{ nm}$) and, to
194 a lesser extent, $\{020\}$ ($2\theta = 32.7^\circ$ and $d = 0.275 \text{ nm}$) for
195 the orthorhombic FeB phase, and $\{002\}$ ($2\theta = 42.7^\circ$ and
196 $d = 0.212 \text{ nm}$) for the tetragonal Fe_2B phase. The change in
197 intensities of those reflections with increasing distance 198

Fig. 2 Backscattered electron images of boride layers formed at the steel-boron interface at a temperature of $950 \text{ }^\circ\text{C}$. The darker layer bordering the boriding agent is the FeB phase, while the brighter layer adjacent to the steel base is the Fe_2B phase



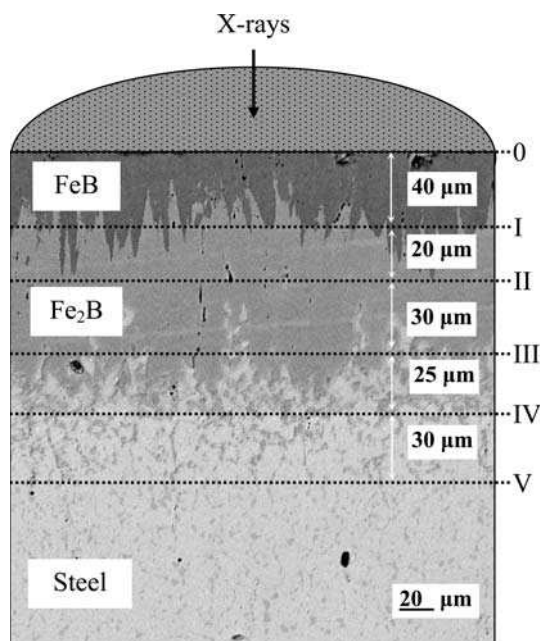
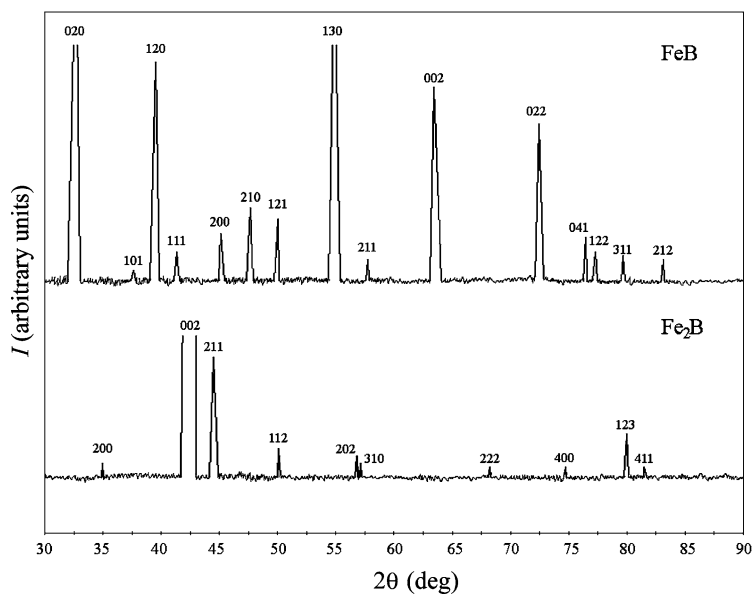


Fig. 3 Scheme of X-ray diffraction experiments

199 from the surface of a borided steel Tablet is illustrated in
200 Table 3. Note that with isotropic microcrystalline samples
201 the strongest reflections are {111}, {200} and {210} for
202 FeB and {211} for Fe₂B.

203 As seen from Table 3, the larger orientation order is
204 characteristic of the inner portions of both boride layers
205 compared to their near-interface portions, in agreement
206 with findings of other researchers [1, 14, 15]. This is easily
207 explainable because near-interface portions of any boride
208 layer are less equilibrated compared to its inner portions.

Fig. 4 X-ray diffraction patterns of the FeB (section 0, see Fig. 3) and Fe₂B (section II) phases formed at the steel-boron interface. Boriding conditions: temperature 950 °C, reaction time 21600 s (6 h)



Therefore, near-interface crystals have less time to align in
the preferred direction. The process of formation of the
boride-layer texture has been discussed in detail, for
example, by Voroshnin and Lyakhovich [1] and recently by
Martini et al. [15].

X-ray investigations were followed by EPMA measurements (Table 4). Sections 0 of a borided steel sample corresponded to the FeB phase. Section I crossed both the FeB and Fe₂B phases (Fig. 6 and Table 4). Section II crossed the Fe₂B phase (Fig. 7 and Table 4). Section III was the Fe₂B phase and the steel base in approximately equal amounts. The microstructure of section IV consisted of the steel base with fine inclusions of the Fe₂B phase and an Fe–Cr phase containing 33–53 at.% chromium (Fig. 8 and Table 4). Section V was entirely the steel base of nominal composition.

The FeB and Fe₂B phases dissolve considerable amounts of chromium (Tables 4 and 5). Its distribution within the boride layers is rather irregular (Fig. 9), due probably to non-equilibrium conditions of layer formation. The average chromium content is 8 at.% in the (Fe,Cr)B layer and 9 at.% in the (Fe,Cr)₂B layer. These values agree fairly well with literature ones [14].

Microhardness of boride phases

Microhardness, HV, of the outer (Fe,Cr)B layer was found to be 17.9 ± 1.5 GPa, while that of the inner (Fe,Cr)₂B layer 16.1 ± 0.9 GPa. For the steel base, its value is 5.9 ± 0.3 GPa.

A plot of microhardness values against distance across reacting phases is shown in Fig. 10. Microhardness is practically constant within both boride layers and slightly

Table 1 Comparison of literature and our experimental X-ray data (*d*-spacing and peak intensities) for the FeB phase (section 0, see Fig. 3) formed at the steel-boron interface at 950 °C and a reaction time of 21600 s (6 h)

Literature data [13]			Our experimental data		
HKL	<i>d</i> (nm)	I*	2θ(deg)	<i>d</i> (nm)	I
110	0.326	m	27.5	0.3244	vw
020	0.275	s	32.7	0.2738	vs
101	0.240	s	37.5	0.2398	vw
120	0.228	s	39.7	0.2271	s
111	0.219	vs	41.3	0.2181	w
200; 021	0.201	vs	45.2	0.2006	m
210	0.190	vs	47.8	0.1903	s
121	0.181	s	50.0	0.1818	s
130	0.167	s	55.1	0.1667	vs
211	0.160	s	57.5	0.1603	w
002	0.148	m	63.2	0.1471	vs
022	0.1303	m	72.7	0.1301	s
041	0.1249	m	76.6	0.1244	m
122	01239	vs	77.3	0.1234	w
311	0.1199	m	80.6	0.1192	w
212	0.1166	vs	83.1	0.1162	w

*Intensity; vw—very weak; w—weak; m—medium; s—strong; vs—very strong

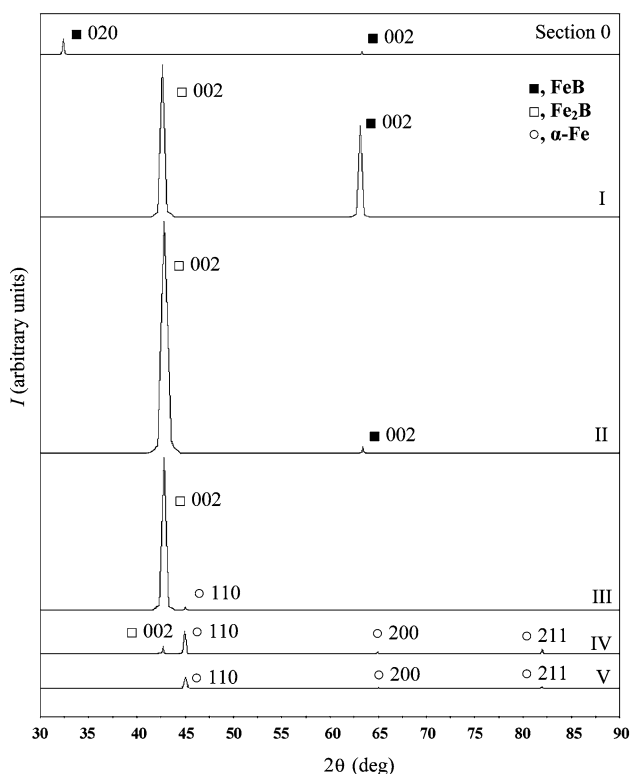


Fig. 5 Most intensive peaks of X-ray diffraction patterns taken from different plain-view sections of a steel sample borided at 950 °C for 21600 s (6 h) (see also Fig. 3 and Table 3)

diminishes (by about 0.2 GPa) in the steel base with increasing distance in the range 0–500 μm from the inner boride layer. 240
241
242

Layer-growth kinetics 243

Compared to other boriding agents mentioned in Introduction, mixtures of amorphous boron and KBF₄ allow much thicker and more regular boride layers to be obtained under similar conditions of temperature and time. In the presence of BF₃ and other volatile boron-containing compounds, the reaction between steels and boron starts simultaneously over the whole interface. With coarse-grained crystalline boron in the absence of any activator, island-like layers are usually formed, even at a considerable reaction time [1]. In the present case, continuous boride layers arose on the steel surface soon (40–60 s) after the start of the boriding procedure. Note that the gas phase only initiates the reaction, while the further growth of boride layers is a solid-state process. 244
245
246
247
248
249
250
251
252
253
254
255
256
257

After compact layers of both borides have formed, their subsequent diffusional growth is due to two partial chemical reactions (Fig. 11) 258
259
260



and 262

Table 2 Comparison of literature and our experimental X-ray data (d -spacing and peak intensities) for the Fe₂B phase (section II, see Fig. 3) formed at the steel-boron interface at 950 °C and a reaction time of 21600 s (6 h)

Literature data [13]			Our experimental data		
HKL	d (nm)	I*	2θ (deg)	d (nm)	I
200	0.256	vw	35.4	0.2536	vw
002	0.212	w	42.7	0.2117	vs
211	0.201	vs	44.8	0.2022	s
112	0.183	m	49.6	0.1838	w
202	0.163	m	56.4	0.1631	w
310	0.161	m	57.6	0.1600	vw
222	0.1371	w	68.0	0.1379	vw
400	0.1277	m	73.7	0.1285	vw
123	0.1202	s	80.0	0.1199	w
411	0.1187	m	81.0	0.1187	vw

*Intensity; vw—very weak; w—weak; m—medium; s—strong; vs—very strong



264 The growth kinetics of compound layers are usually
265 treated using parabolic equations of the type $x^2 = 2k_1t$,
266 where x is the layer thickness, k_1 is the layer growth-rate
267 constant and t is time [9, 16, 17]. For sufficiently thick
268 layers, such equations produce a quite satisfactory fit to the
269 experimental data (Fig. 12 and Table 6).

270 In fact, however, growth kinetics of the FeB and Fe₂B
271 layers at the diffusional stage of their formation are
272 somewhat more complicated and can alternatively be de-
273 scribed by a system of two non-linear equations [10, 18–
274 21]

$$\frac{dx}{dt} = \frac{k_B}{x} - \frac{rg k_{Fe}}{p y} \quad (2.1)$$

$$276 \frac{dy}{dt} = \frac{k_{Fe}}{y} - \frac{q k_B}{sg x} \quad (2.2)$$

278 where x is the FeB layer thickness, y is the Fe₂B layer
279 thickness, k_B is the FeB layer growth-rate constant, k_{Fe}
280 is the Fe₂B layer growth-rate constant, g is the ratio of the
281 molar volumes of the FeB and Fe₂B compounds, $p = q = r$
282 = 1 and $s = 2$ (factors from the chemical formulae of FeB
283 and Fe₂B).

284 Under conditions of diffusion control, both boride layers
285 thicken at their common interface 2, as shown in Fig. 11.
286 The FeB layer grows at the expense of diffusion of the
287 boron atoms across its bulk and their subsequent reaction
288 with the Fe₂B compound. As a result, its thickness in-
289 creases during dt by dx_{B_2} . The Fe₂B layer grows at the
290 expense of diffusion of the iron atoms across its bulk and
291 their further reaction with the FeB compound. During the
292 same time dt , its thickness increases by dy_{Fe_2} . Since the
293 FeB and Fe₂B compounds are consumed in the formation
294 of each other, the thickness of the FeB layer simulta-
295 neously decreases by dx_- , while that of the Fe₂B layer by
296 dy_- . The net change of the FeB layer thickness during dt is

Table 3 X-ray diffraction data showing preferential directions of growth for the FeB and Fe₂B phases formed at the steel-boron interface at 950 °C and a reaction time of 21600 s (6 h)

Phase	HKL	d (nm)	Peak intensity (arbitrary units)					
			0*	I	II	III	IV	V
FeB	020	0.275	203					
	002	0.148	55	1075	93			
Fe ₂ B	002	0.212		1780	2700	1730	35	
α -Fe	110	0.201				54	95	136
	200	0.143					13	15
	211	0.117					25	27

*Serial numbers of appropriate sections of a borided Tablet sample by a plane parallel to its flat surface (section 0, I and so on, deeper into the sample bulk, see Fig. 3).

Table 4 Average Fe, Cr and B contents of reacting phases, found by EPMA measurements on X-ray diffraction samples (see also Figs. 3, 6–8)

Section	Region	Content (at.%)			Phase
		Fe	Cr	B	
I	Darker in Fig. 6	42.0	8.1	49.9	(Fe,Cr) ₂ B
		41.6	7.5	50.9	
		43.5	8.2	48.3	
		41.3	8.7	50.0	
	Brighter in Fig. 6	42.3	9.3	48.4	
		58.6	9.1	32.3	
		56.1	9.7	34.2	
		55.5	10.4	34.1	
II	Brighter in Fig. 7	57.1	10.4	32.5	(Fe,Cr) ₂ B
		55.8	9.3	34.9	
		53.6	11.9	34.5	
		54.9	10.8	33.3	
	Darker in Fig. 7	55.0	10.9	34.1	
		39.1	11.3	49.6	
		39.4	8.8	51.8	
		40.9	10.5	48.6	
IV	Brighter in Fig. 8	85.6	14.4	0.0	Steel base
		83.3	16.7	0.0	
		86.2	13.8	0.0	
	Darker in Fig. 8	34.9	29.4	35.7	
		43.0	27.3	29.7	
		40.3	25.3	34.3	
	Grayish in Fig. 8	61.7	38.3	0.0	
		66.8	33.2	0.0	
V	Brighter in Fig. 8	44.8	55.2	0.0	
		86.1	13.9	0.0	
		84.7	15.3	0.0	
		85.7	14.3	0.0	

Boriding conditions: temperature 950 °C, reaction time 21600 s (6 h)

297 the difference between dx_{B_2} and dx_- , while that of the Fe_2B
 298 layer thickness is the difference between dy_{Fe_2} and dy_- .
 299 Therefore, Eqs. (2.1) and (2.2) contain two terms on their
 300 right-hand parts.

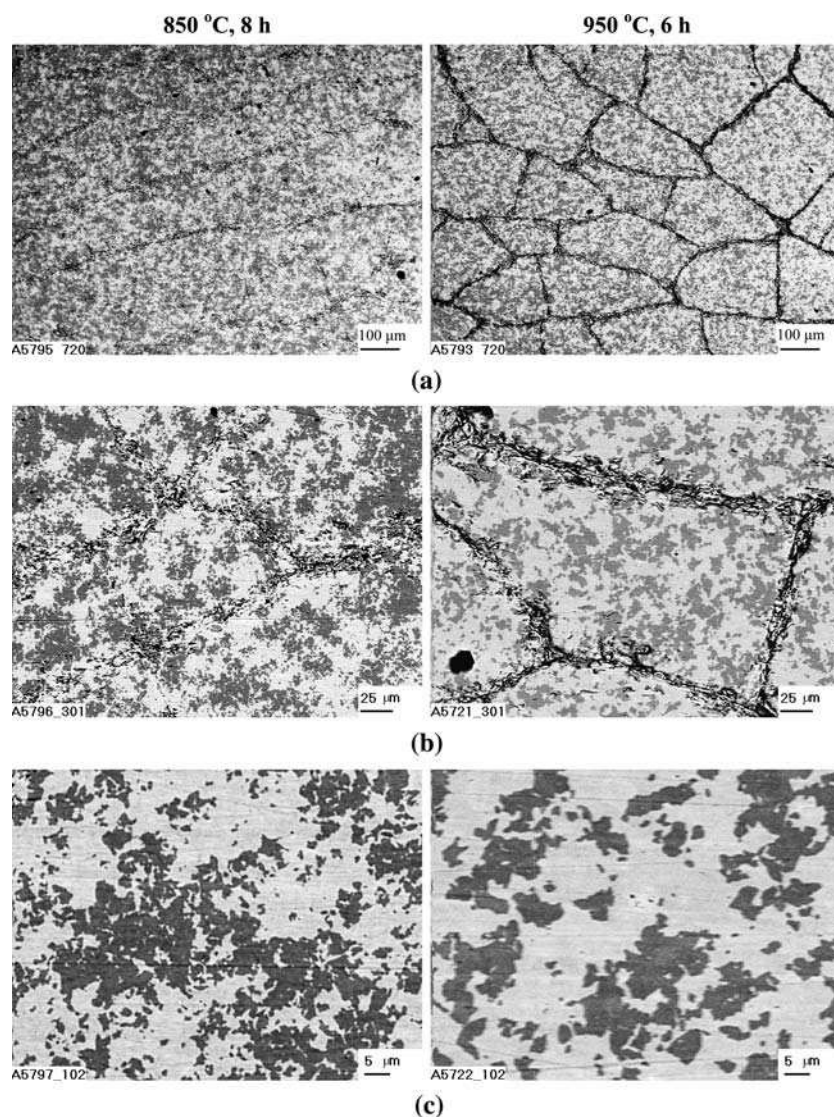
301 Even though both boride layers are often considered to
 302 grow at the expense of diffusion of the single component
 303 boron across their bulks, it is hardly possible with compact
 304 layers having no macrodefects and therefore growing by
 305 the volume-diffusion mechanism. During diffusional
 306 growth, by definition, diffusion across the layer bulks is the
 307 rate-determining step, the interface reactions being very
 308 fast. It means that all the boron atoms reaching interface 2
 309 react with Fe_2B to form FeB at that interface. Since under
 310 conditions of diffusion control the ability of interface 2 to
 311 combine those atoms exceeds their diffusional transport
 312 across the FeB layer (slow diffusion followed by fast

reaction), none of them can diffuse further to interface 3
 and react with Fe to form Fe_2B : $B_{dif} + 2Fe = Fe_2B$.

This reaction can only take place either under conditions
 of reaction control when the flux of boron atoms from the
 initial B-containing phase is sufficient for both boride
 layers to grow (for more detail, see Ref. [10]) or if the FeB
 layer is non-protective due to the presence of cracks and
 other macrodefects. Reaction-controlled growth is only
 typical of thin compound layers ($< 1 \mu m$ thick). The FeB
 layer was compact and therefore non-permeable to BF_3 and
 other gases. Hence, neither of these growth mechanisms
 could be operative with the borides layers investigated.

From a chemical viewpoint, it must thus be clear that the
 diffusional growing FeB layer itself can by no means be a
 source of boron atoms for the Fe_2B layer to grow. Suppose
 that two FeB molecules decompose at interface 2 to yield

Fig. 6 Plain-view micrographs (backscattered electron images at different magnification) corresponding to section I (see Fig. 3). The darker phase is FeB, while the brighter phase is Fe₂B. Black spots are holes. Penetration of boron along grain boundaries is worth noting



329 one molecule of Fe₂B and one diffusing boron atom: 2FeB
 330 = Fe₂B + B_{dif}. However, this boron atom will be unable to
 331 diffuse from interface 2 to interface 3 because under con-
 332 ditions of diffusion control the Fe₂B surface is undersat-
 333 urated with boron atoms and therefore it is immediately
 334 combined at interface 2 according to the reaction B_{dif} +
 335 Fe₂B = 2FeB. The net result of those reactions is seen to be
 336 zero. On the contrary, under conditions of reaction control
 337 the Fe₂B surface bordering the FeB layer is oversaturated
 338 with boron atoms and therefore part of them (not combined
 339 into the FeB phase at interface 2) readily diffuse further to
 340 interface 3 and react with iron atoms to form Fe₂B. As the
 341 only source of boron atoms for both layers to grow is the
 342 boriding mixture (B and KBF₄), it is clear that sooner or
 343 later the flux of boron atoms, diminishing as the FeB layer
 344 thickens, becomes only sufficient for the FeB layer itself to
 345 grow, whereas the faraway Fe₂B layer must stop growing.

Similarly, all the iron atoms diffusing across the Fe₂B
 layer are combined into Fe₂B by their reaction with FeB at
 interface 2. Hence, iron atoms cannot take part in the for-
 mation of the FeB layer at interface 1. Thus, under con-
 ditions of diffusion control both boride (and any other
 compound) layers only grow at their common interface by
 pushing each other in opposite directions.

This conclusion is usually overlooked, if the process of
 formation of compound layers is treated without writing
 the equations of chemical reactions proceeding at the layer
 interfaces. In fact, at the diffusional stage of layer forma-
 tion each of two compound layers without defects can grow
 only at the expense of diffusion of the atoms of a neigh-
 boring initial phase.

Even though grain-boundary diffusion might also con-
 tribute the layer-growth process, its contribution appears to be
 much less compared to that of volume diffusion in view of the

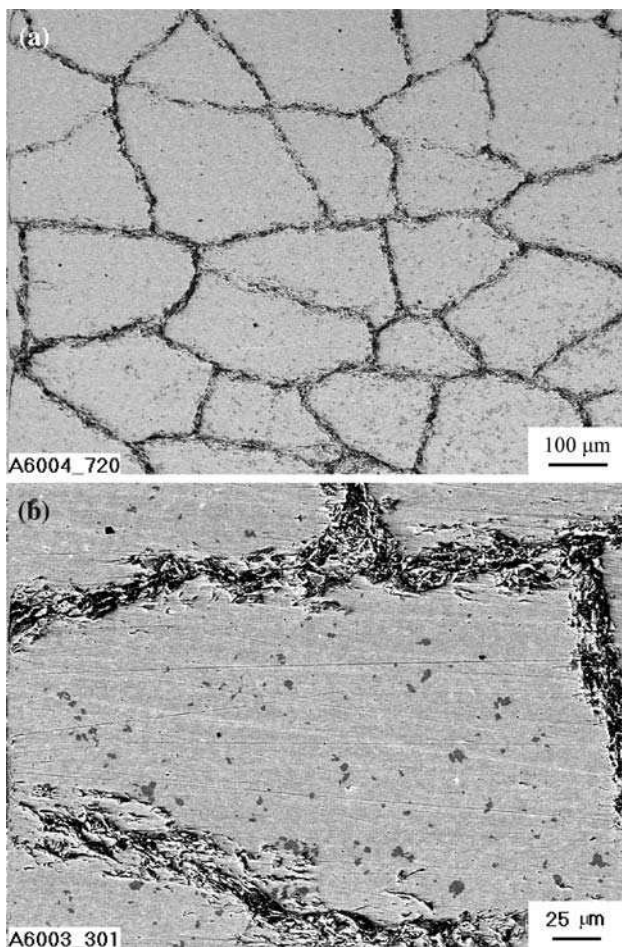


Fig. 7 Plain-view micrographs (backscattered electron images at different magnification) corresponding to section II (see Fig. 3). The main phase is Fe_2B (bright). Inclusions of FeB (darker) are fine and rare. Penetration of boron along grain boundaries is worth noting

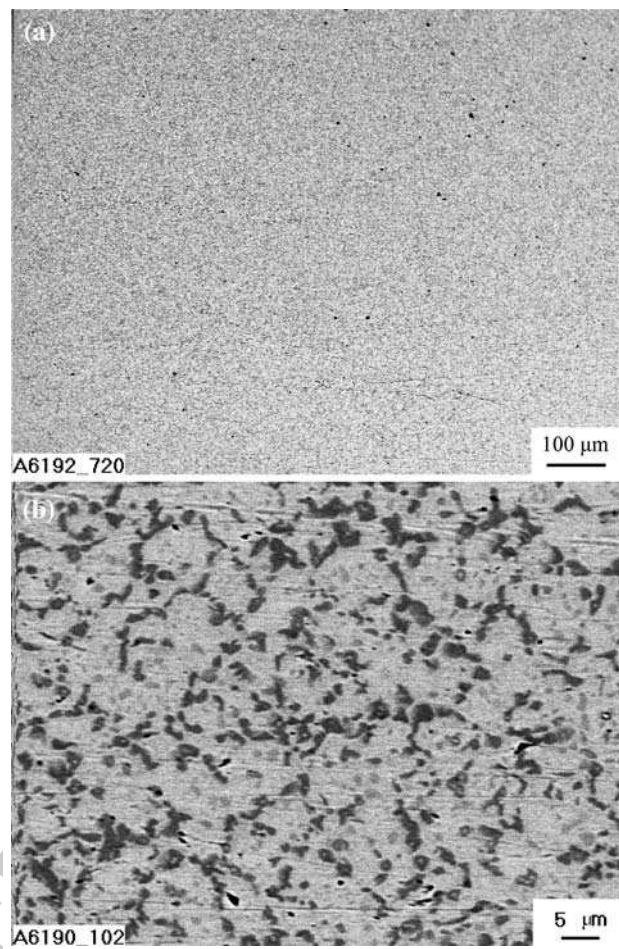


Fig. 8 Plain-view micrographs (backscattered electron images at different magnification) corresponding to section IV (see Fig. 3). The brighter phase is the steel base, while the darker phase is Fe_2B . The steel base is non-homogeneous. Its grayish regions are enriched in chromium

363 coarse-grained structure of both layers. Therefore, in spite of
364 the considerable difference in values of grain-boundary dif-
365 fusion and volume diffusion coefficients, the flux of diffusing
366 atoms along grain boundaries could hardly be large.

367 An obvious criterion of the applicability of Eqs. (2) for
368 treating the diffusional layer-growth kinetics is the constancy of
369 k_B and k_{Fe} over a given range of time, as is the case with boride
370 layers (Table 6). The value of g necessary for calculations of k_B
371 and k_{Fe} was estimated from the densities, $\rho_1 = 6.70 \times 10^3 \text{ kg m}^{-3}$
372 and $\rho_2 = 7.34 \times 10^3 \text{ kg m}^{-3}$, of the FeB and Fe_2B
373 compounds [1] and their molecular masses, $M_1 = 66.65 \text{ g mol}^{-1}$
374 and $M_2 = 122.49 \text{ g mol}^{-1}$: $g = M_1 \rho_2 / M_2 \rho_1 = 0.60$.
375

376 The derivatives were found from the experimental layer
377 thickness-time dependences by the numerical three-point
378 method using a conventional computer program (linear
379 approximation). To find a derivative for a given experi-
380 mental point, (x_i, t_i) , like those on left-hand plots of
381 Fig. 12, data for two neighboring points, (x_{i-1}, t_{i-1}) and

(x_{i+1}, t_{i+1}) , were also used. Left-hand and right-hand
382 derivatives, $(x_i - x_{i-1}) / (t_i - t_{i-1})$ and $(x_{i+1} - x_i) / (t_{i+1} - t_i)$,
383 were first found for this point and a mean value was then
384 calculated. The derivatives could thus be found for all
385 experimental points, excepting clearly end ones, for which
386 a neighboring point is lacking.
387

388 As seen in Table 6, the results of calculations of k_B and
389 k_{Fe} are strongly dependent upon a scatter of experimental
390 points. To avoid this, approximation of experimental data
391 with any suitable analytical function is therefore advisable.
392 For example, the use of parabolic relations to approximate
393 the layer thickness-time dependences and then to find the
394 derivatives yields another set of values of k_B and k_{Fe}
395 (Table 7). Since the experimental $x-t$ dependences become
396 smoothed as a result of this procedure (solid lines on left-
397 hand plots of Fig. 12), all values of k_B thus found are
398 identical. The same applies to k_{Fe} . Comparing these with
399 the average values of k_B and k_{Fe} found numerically from

Table 5 EPMA data for the steel-boron diffusion zone. Temperature 950 °C, reaction time 21600 s (6 h)

Phase	Place of measurement	Content (at.%)			Remarks
		Fe	Cr	B	
	At distance l away from the steel-boride layer interface				
Steel	$l = -150 \mu\text{m}$	86.8	13.2	0.0	< Fe >
	-80	78.5	17.8	3.7	
	-50	87.0	13.0	0.0	
	-20	89.8	10.1	0.0	
	-10	82.7	10.7	6.6	
Inner boride layer	10	56.5	9.2	34.3	(Fe,Cr) ₂ B
	20	59.2	9.0	31.8	
	30	54.8	10.7	34.6	
	40	60.9	9.2	30.0	
	50	61.7	6.4	31.9	
Outer boride layer	60	40.9	7.4	51.7	(Fe,Cr)B
	70	43.3	8.6	48.1	
	80	42.1	7.2	50.7	
	90	43.3	8.5	48.2	

400 the experimental points, it may be concluded that both sets
401 of the constants agree fairly well, providing evidence for
402 the validity of the analytical treatment employed.

403 The temperature dependence of the layer growth-rate
404 constants is described in the 850–950 °C range by the
405 following equations of the Arrhenius type

$$K = K_0 \exp(-E/RT) \quad (3)$$

407 where K stands for any layer growth-rate constant, E is the
408 activation energy, R is the gas constant and T is the
409 absolute temperature (Fig. 10):

$$k_1 = 1.46 \times 10^{-7} \exp(-149.4 \text{ kJ mol}^{-1}/RT) \text{ m}^2 \text{ s}^{-1}$$

for the FeB layer,

$$k_1 = 7.87 \times 10^{-9} \exp(-116.4 \text{ kJ mol}^{-1}/RT) \text{ m}^2 \text{ s}^{-1}$$

for the Fe₂B layer,

$$k_1 = 1.36 \times 10^{-7} \exp(-132.8 \text{ kJ mol}^{-1}/RT) \text{ m}^2 \text{ s}^{-1}$$

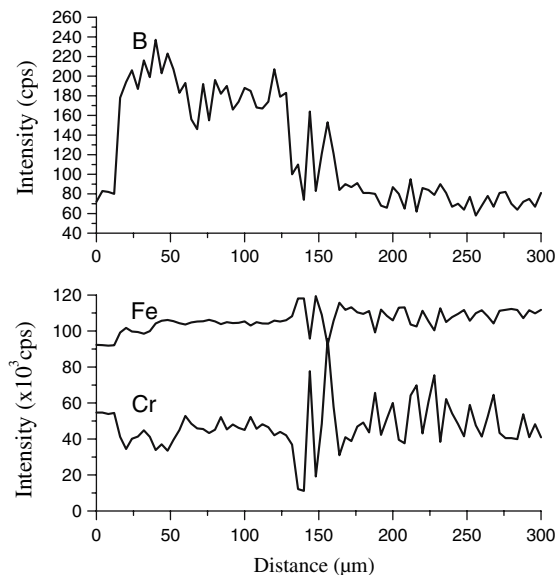
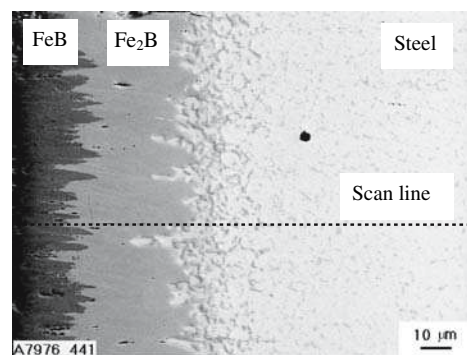
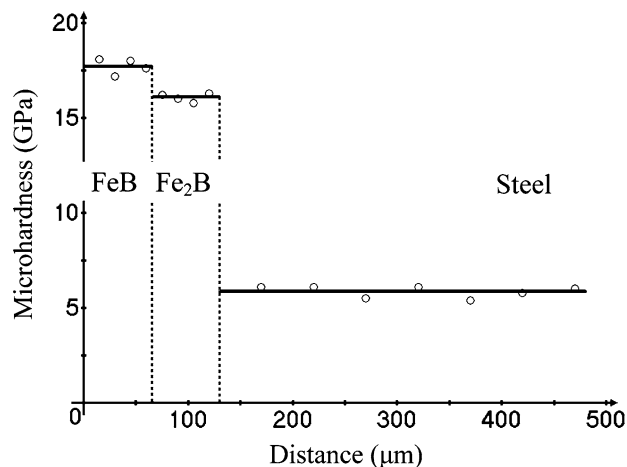
for both boride layers,

$$k_B = 4.40 \times 10^{-7} \exp(-142.2 \text{ kJ mol}^{-1}/RT) \text{ m}^2 \text{ s}^{-1},$$

$$k_{Fe} = 1.24 \times 10^{-7} \exp(-124.3 \text{ kJ mol}^{-1}/RT) \text{ m}^2 \text{ s}^{-1}.$$

411 Degradation of boride layers during annealing
412 in the absence of boriding media

413 Annealing of a borided steel sample (Fig. 14a) in vacuum
414 in the absence of the boriding mixture (B and KBF₄) results

**Fig. 9** Microstructure of the transition zone between a commercial 13%Cr steel and boron and concentration profiles of Fe, Cr and B. Boriding conditions: temperature 950 °C, reaction time 21600 s (6 h)**Fig. 10** A plot of microhardness, HV, against distance within reacting phases. Boriding conditions: temperature 950 °C, reaction time 21600 s (6 h)

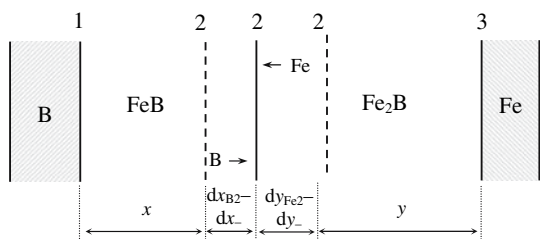


Fig. 11 Schematic diagram to illustrate the growth process of two boride layers under conditions of diffusion control. Both layers thicken at their common interface 2. No reactions take place at interfaces 1 and 3 in view of the lack of appropriate diffusing atoms

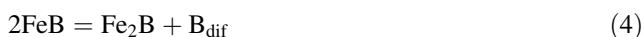
$$B_{dif} + 2Fe = Fe_2B \tag{5}$$

taking place at the FeB–Fe₂B and the Fe₂B–steel interfaces, respectively.

It should be noted that the growing and non-growing FeB layers behave quite differently. Unlike the diffusionally growing FeB layer, not sharing boron atoms with its neighbor Fe₂B, the non-growing one not only shares those atoms with Fe₂B but also forms an additional molecule of Fe₂B as a result of its own decomposition (for more examples of such a behavior of compound layers, see Ref. [10]).

As seen in Fig. 14b, c, the FeB layer, initially compact and around 50 μm thick, disintegrates during vacuum annealing into separate grains and after a 12 h hold at 950 °C disappears almost completely. Grain-boundary diffusion appears to play a significant, if not decisive, role in this process because usually compound layers are consumed as a whole at their interfaces with adjacent

415 in a decrease of the thickness of the FeB layer and an
416 appropriate increase of the thickness of the Fe₂B layer due
417 to the reactions



419 and

Fig. 12 Plots of layer thickness (left) and squared layer thickness (right) against time for (a) both boride layers, (b) the FeB layer and (c) the Fe₂B layer at a temperature of 850 °C (line 1), 900 °C (line 2) and 950 °C (line 3)

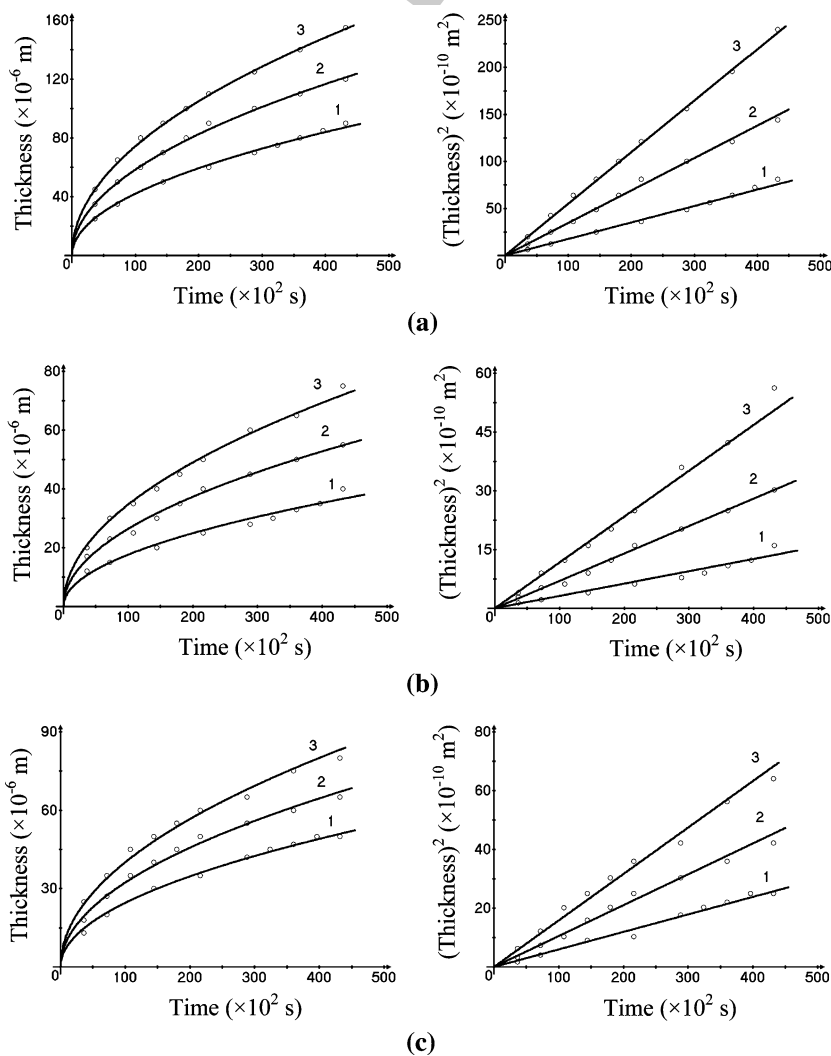


Table 6 Thickness and growth constants of the FeB and Fe₂B layers formed at the steel-boron interface

Temperature (°C)	Time ($\times 10^2$ s)	x ($\times 10^{-6}$ m)			k_1 ($\times 10^{-14}$ m ² s ⁻¹)			k ($\times 10^{-13}$ m ² s ⁻¹)*	
		Total	FeB	Fe ₂ B	Total	FeB	Fe ₂ B	k_B	k_{Fe}
850	36	25	12	13	8.7	2.0	2.3		
	72	35	15	20	8.5	1.6	2.8	1.54	3.13
	144	50	20	30	8.7	1.4	3.1	0.94	2.01
	216	60	25	35	8.3	1.5	2.8	0.94	1.88
	288	70	28	42	8.5	1.4	3.1	1.03	2.23
	324	75	30	45	8.7	1.4	3.1	1.19	2.46
	360	80	33	47	8.9	1.5	3.1	1.31	2.56
	396	85	35	50	9.1	1.5	3.2	1.53	2.83
	432	90	40	50	9.4	1.9	2.9		
900	36	35	17	18	17.0	4.0	4.5		
	72	50	23	27	17.4	3.7	5.1	2.08	3.56
	108	60	25	35	16.7	2.9	5.7	1.84	3.72
	144	70	30	40	17.0	3.1	5.6	2.38	4.37
	180	80	35	45	17.8	3.4	5.6	2.78	4.91
	216	90	40	50	18.8	3.7	5.8	3.17	5.46
	252	100	45	55	17.4	3.5	5.3	3.57	6.00
	288	110	50	60	16.8	3.5	5.0	2.98	4.91
	360	120	55	65	16.7	3.5	4.9		
950	36	45	20	25	28.1	5.6	8.7		
	72	65	30	35	29.3	6.3	8.5	4.02	6.60
	108	80	35	45	29.6	5.7	9.3	3.30	6.03
	144	90	40	50	28.1	5.6	8.7	3.17	5.46
	180	100	45	55	27.8	5.6	8.4	3.57	6.00
	216	110	50	60	28.0	5.8	8.3	3.60	5.80
	288	125	60	65	27.1	6.3	7.3	3.57	5.32
	360	140	65	75	27.2	5.9	7.8	1.77	2.98
	432	155	75	80	27.8	6.5	7.4		

*Mean values: $k_B = (1.21 \pm 0.36) \times 10^{-13}$ m² s⁻¹ and $k_{Fe} = (2.44 \pm 0.62) \times 10^{-13}$ m² s⁻¹ at 850 °C, $k_B = (2.68 \pm 0.69) \times 10^{-13}$ m² s⁻¹ and $k_{Fe} = (4.70 \pm 0.86) \times 10^{-13}$ m² s⁻¹ at 900 °C and $k_B = (3.29 \pm 0.83) \times 10^{-13}$ m² s⁻¹ and $k_{Fe} = (5.45 \pm 0.97) \times 10^{-13}$ m² s⁻¹ at 950 °C.

Table 7 Values of layer growth-rate constants found from a parabolic relation, k_1 , and from Eqs. (2), k

Temperature (°C)	k_1 ($\times 10^{-14}$ m ² s ⁻¹)			k ($\times 10^{-13}$ m ² s ⁻¹) from experimental points		k ($\times 10^{-13}$ m ² s ⁻¹) from approximated dependences	
	total	FeB	Fe ₂ B	k_B	k_{Fe}	k_B	k_{Fe}
850	8.8	1.6	3.0	1.21	2.44	1.04	2.01
900	17.3	3.5	5.3	2.68	4.70	2.17	3.74
950	28.1	5.9	8.3	3.29	5.45	3.61	5.96

438 layers, with their compactness retaining and their thick-
439 ness decreasing.

440 Abrasive wear resistance of boride layers

441 Boriding the steel Tablets for abrasive wear resistance
442 tests was performed at 950 °C for 6 h, producing the

(Fe,Cr)B and (Fe,Cr)₂B layers of close thickness (about 443 110 μ m in total). Six consecutive tests were carried out 444 on each borided steel sample, with each test along a fresh 445 track (27.0 m long) on emery paper. The results obtained 446 are presented in Table 8, where the data for a non-borided 447 steel sample (one test, 27.0 m) are also given for com- 448 parison. 449

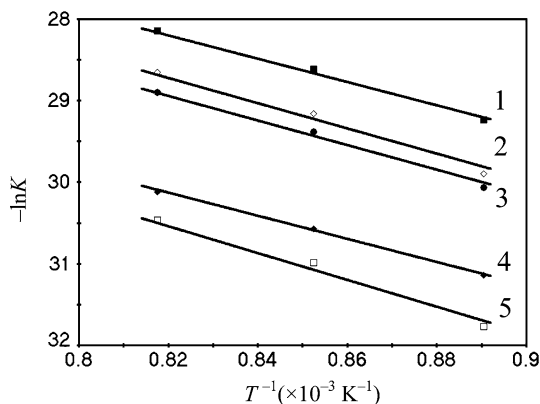


Fig. 13 The temperature dependence of the layer growth-rate constants, K : 1, k_{Fe} ; 2, k_B ; 3, k_1 for both boride layers; 4, k_1 for Fe_2B ; 5, k_1 for FeB

450 The wear resistance of the $(Fe,Cr)B$ layer, found from
 451 mass loss measurements, is about 25 times greater than that
 452 of the alloy base. Deeper portions of $(Fe,Cr)B$ coatings
 453 display a higher wear resistance compared to near-surface
 454 ones due to a more profound texture and a much less
 455 amount of cracks. The wear resistance of the inner
 456 $(Fe,Cr)_2B$ layer is around 15 times greater than that of the
 457 steel base.

458 Comparing the wear resistance of the outer boride
 459 coating on the surface of the steel and Fe–Cr alloys con-
 460 taining 10 and 25% Cr [22], it may be concluded that its

value for the steel and an Fe–10% Cr alloy are rather close,
 with the coating on the steel surface being about 15% more
 resistant than that on the alloy surface. The FeB coating on
 both materials is much less resistant (by an order of mag-
 nitude) than that on an Fe–25% Cr alloy. Most probably, it
 is due to structural or morphological rather than composi-
 tional reasons.

Conclusions

Two boride phases FeB and Fe_2B occur as separate
 layers at the interface between a commercial 13%Cr
 steel (40×13) and a mixture of amorphous boron
 with 5% KBF_4 at 850–950 °C and reaction times up to
 12 h. The average content of chromium is around 8 at.%
 in the outer FeB layer and 9 at.% in the inner Fe_2B
 layer.

The characteristic feature of both layers is a pronounced
 texture. The strongest reflections are $\{002\}$ and $\{020\}$ for
 the orthorhombic FeB phase and $\{002\}$ for the tetragonal
 Fe_2B phase.

Diffusional growth kinetics of the boride layers are
 close to parabolic. Alternatively, layer-growth kinetics
 can be described by a system of non-linear differential
 equations, also producing a good fit to the experimental
 data.

Fig. 14 Backscattered electron images at different
 magnification illustrating the process of degradation of boride
 layers during vacuum annealing at a temperature of 950 °C in
 the absence of the boriding
 mixture: (a) as-received
 condition, (b) 6 h annealing
 and (c) 12 h annealing

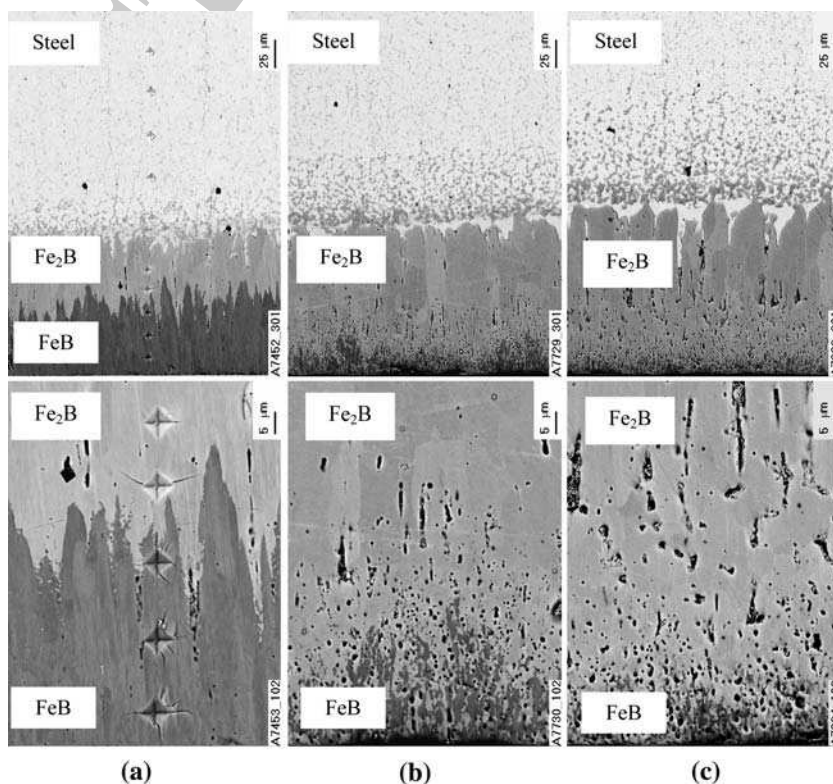


Table 8 Results of abrasive wear resistance tests of borided steel samples. Boriding conditions: temperature 950 °C, reaction time 21600 s (6 h). Six consecutive tests (each along a fresh track, 27.0 m long) were carried out on each of three borided samples. Mean values for each test are presented (deviation $\pm 15\%$). For comparison, one test (27.0 m) was performed on a non-borided steel sample

Serial test number	Δm (g)*	$\Delta m_{\text{steel}} : \Delta m_{\text{boride}}$	Δh (mm)	Phase
1	0.02817	11.8	0.025	(Fe,Cr)B
2	0.01290	25.8	0.015	(Fe,Cr)B
3	0.01857	17.9	0.020	(Fe,Cr)B + (Fe,Cr) ₂ B
4	0.02117	15.7	0.025	(Fe,Cr) ₂ B
5	0.03977	10.0	0.035	(Fe,Cr) ₂ B + steel base
6	0.05400	6.6	0.045	(Fe,Cr) ₂ B + steel base
1	0.3329	–	0.40	Non-borided sample

* Δm and Δh are changes in mass and height, respectively, of samples.

485 Annealing of a borided steel sample in the absence of
486 boriding media causes the disappearance of the FeB layer.
487 Grain-boundary diffusion appears to play a significant role
488 in this process.

489 Microhardness values are 17.9 ± 1.5 GPa for the FeB
490 layer, 16.1 ± 0.9 for the Fe₂B layer and 5.9 ± 0.3 GPa for
491 the steel base. Microhardness is practically constant within
492 both boride layers.

493 The abrasive wear resistance of the FeB layer, found
494 from mass loss measurements, is approximately 25 times
495 greater than that of the steel base. The Fe₂B layer yields
496 about a 15-fold increase in wear resistance of steel
497 samples.

498 **Acknowledgements** This investigation was supported in part by the
499 STCU grant No. 2028. The author is grateful to V. G. Khoruzha, V. R.
500 Sidorko, K. A. Meleshevich and A. V. Samelyuk for their help in
501 conducting the experiments and carrying out the necessary analyses.

502 References

- 503 1. Voroshnin LG, Lyakhovich LS (1978) Borirovaniye stali. Met-
504 allurgiya, Moskwa, (in Russian)
- 505 2. Kunst H, Schroll H, Luetje R, Wittel K, Lugscheider E, Weber T,
506 Eschnauer HR, Raub C (1991) In: Ullmann's Encyclopedia of
507 Industrial Chemistry, vol A16. Verlag Chemie, Weinheim, p 427
- 508 3. Sinha AK (1982) Boriding (Boronizing). In: Sinha AK (ed)
509 Metals Handbook. ASM International, Metals Park OH, p 844
- 510 4. Hansen M, Anderko K (1958) Constitution of binary alloys, 2nd
511 edn. McGraw-Hill, New-York, p 249

- 512 5. Vol AE (1962) Stroeniye i svoystva dvoynikh metallicheskih
513 system, vol 1. Fizmatgiz, Moskwa, p 679 (in Russian)
- 514 6. Massalski TB, Murray JL, Bennett LH, Baker H (eds) (1986)
515 Binary Alloy Phase Diagrams, vol 1. American Society of Met-
516 als, Metals Park OH, p 351
- 517 7. Okamoto H (2004) J Phase Equilib Diffusion 25:297–298
- 518 8. Brandstötter J, Lengauer W (1997) J Alloys Compd 262–
519 263:390–396
- 520 9. Gurov KP, Kartashkin BA, Ugaste YuE (1981) Vzaimnaya dif-
521 fuziya v mnogofaznikh metallicheskih sistemakh. Nauka, Mos-
522 kwa, (in Russian)
- 523 10. Dybkov VI (2002) Reaction diffusion and solid state chemical
524 kinetics. The IPMS Publications, Kyiv, (free access at [http://](http://users.i.com.ua/~dybkov/V)
525 users.i.com.ua/~dybkov/V)
- 526 11. Voroshnin LG (1981) Borirovaniye promyshlennikh staley i
527 chugunov. Belarus, Minsk, (in Russian)
- 528 12. Dybkov VI, Lengauer W, Barmak K (2005) J Alloys Compd
529 398:113–122
- 530 13. Gorelik SS, Rastorguev LN, Skakov YuA (1970) Rentgenogra-
531 ficheskiy i elektronno-opticheskiy analiz, prilozheniya. Metal-
532 lurgiya, Moskwa, p 29 (in Russian)
- 533 14. Carbuicchio M, Palombarini G (1987) J Mater Sci Lett 6:1147–
534 1149
- 535 15. Martini C, Palombarini G, Carbuicchio M (2004) J Mater Sci
536 39:933–937
- 537 16. Seith W (1955) Diffusion in metallen. Springer, Berlin
- 538 17. Hauffe K (1955) Reaktionen in und an festen Stoffen. Springer,
539 Berlin
- 540 18. Arkharov VI (1959) Fiz Metall Metalloved 8:193–204
- 541 19. Schröder B, Leute V (1980) J Phys Chem Solids 41:827–835
- 542 20. Fromhold AT, Sato N (1981) Oxid Metals 16:203–220
- 543 21. Dybkov OV, Dybkov VI (2004) J Mater Sci Lett 39:6615–6617
- 544 22. Dybkov VI, Lengauer W, Barmak K (2005) In: Proc 16th Plansee
545 Seminar, Reutte, Austria, May 31–June 4, 2:999–1009
- 546